A New Handheld Sensor for Measuring Intrinsic Dielectric Properties at 100 to 1000 MHz

J.W. Schultz, *Member, AMTA,*
R. Geryak, *Member, AMTA.*
Compass Technology Group
Alpharetta, GA, USA
john.schultz@compasstech.com

***Abstract*— Traditional fixtures for UHF and VHF measurements of dielectric properties require specimens cut or machined with precision tolerances to avoid air gap errors. They also require significant handling and multi-step calibration procedures, complicating their use in non-laboratory applications. This paper introduces a new, non-traditional, measurement method for obtaining complex dielectric properties at UHF and VHF frequencies. It applies an open-ended stripline sensor in a handheld device that non-destructively measures reflection from a material surface. A novel computational electromagnetic (CEM) inversion methodology is applied to translate from reflection amplitude and phase into complex permittivity or sheet impedance. Because of this CEM inversion, the calibration is a simple one-step process. The CEM inversion method also enables characterization of multilayer structures as well as anisotropic materials. In addition to general principles for the device, example measurements as well as measurement comparisons to conventional dielectric measurement systems are presented.**

I. INTRODUCTION

This paper is concerned with measuring dielectric properties of materials at UHF and VHF frequencies (100 to 1000 MHz). A traditional method for characterization at these frequencies is the coaxial airline, where a toroid shaped specimen is placed within the airline and transmission and/or reflection are measured. Coaxial methods have the advantage of broad band operation and the required specimen sizes are small. However, the requirement to exactly fit a specimen between the inner and outer conductor of a coaxial line makes sample preparation difficult. Imperfections in sample fit lead to air gap errors, which limit the accuracy of the method for dielectric properties. Finally, the radial electric field orientation within a coaxial line limits the ability to characterize anisotropic properties [1].

Another traditional method used at UHF and VHF frequencies is the rectangular waveguide. Like the coaxial line, this technique is also limited by air gap errors. Furthermore, waveguide methods are band limited so that the UHF and VHF frequencies can only be spanned by measuring a sequence of different sized specimens with different waveguide bands. Finally, waveguide width approaches a wavelength in size for operation at the fundamental mode, so a significant amount of material may be required to fill the interior of these larger waveguide fixtures.

Free-space methods have been used at UHF frequencies [2], but the requirement for specimens to be at least two to three wavelengths or larger in dimension make free space increasingly impractical for the longer wavelengths. Capacitive or 'impedance analysis' methods have also seen some success at these frequencies, and they work with small specimen sizes and can span the whole frequency range [3]. However, the capacitive methods require specimens to be within a certain thickness range so that they can be sandwiched between electrodes placed on both sides of a planar sample

In contrast to these traditional techniques, the new method described here uses an open-ended sensor placed against just one side of a specimen. Thus, it can be used on arbitrarily thick materials. In addition, moderately small specimens can be characterized since the sensor is electrically small, with a footprint of less than 10 x 10 cm. The ability to handle smaller specimen sizes is a significant advantage compared to free space or waveguide methods. In addition, the presented sensor can measure non-destructively the local dielectric properties of a larger component, giving it the ability to be used in manufacturing applications without the need for destructive testing or witness coupons. The presented fixture is based on a one-port reflectometer method and employs a miniaturized microwave network analyzer, making the system highly portable. This paper overviews the design and operational principles of the new sensor, as well as the method for obtaining intrinsic dielectric permittivity from the measured reflection data.

Unlike the traditional dielectric material measurement methods, the presented sensor cannot be described with analytical functions for inverting intrinsic properties from the measured scattering parameters. Instead, a computational electromagnetic (CEM) model is used to create a database for translating between reflection coefficients and intrinsic dielectric properties. CEM based inversions are relatively new but provide a route for realizing new types of measurement fixtures that are not possible otherwise [4]. This paper also describes the application of CEM inversion methodology to the new sensor, including strategies for handling highly anisotropic materials with the electrically small sensor. Finally, this paper provides examples of experimental measurements. These measured data are validated against more traditional RF material fixture results.

II. Material Measurement Probe

The idea of an open-ended transmission line for measuring dielectric properties has been around for many decades [5]. These coaxial probes are placed against a flat surface or in a liquid to measure its dielectric properties and these probes have cylindrical geometry with radial electric fields, so they are insensitive to anisotropic material properties. However, many modern engineering materials are anisotropic composites with direction dependent properties. For this reason, the present probe design is based on an open-ended stripline transmission line rather than a cylindrically symmetric coaxial line. Figure 1 shows a notional cross-section of the open-ended stripline geometry. For measurement the open-end of the probe is placed adjacent to a specimen under test. The dominant electric field is in the left-right direction and this probe can measure moderate levels of anisotropy in materials without correction. For extreme levels of anisotropy (e.g. > 3:1), additional procedures are required to improve measurement accuracy. These anisotropy corrections are discussed later in this paper. A low dielectric foam is used in the interior of the sensor to ensure the inner conductor is mechanically supported and centered.

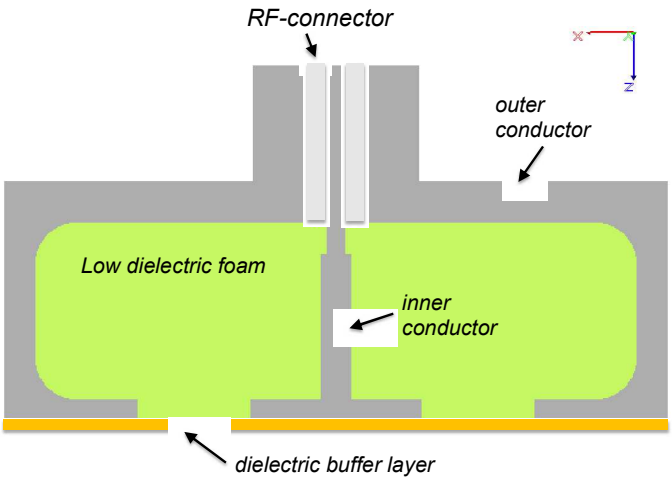

Figure 1. Cross-section of open-ended stripline sensor,

A known drawback to traditional coaxial probe methods is their sensitivity to airgaps between the open end of the probe and the specimen under test. This can be a significant source of measurement error for these conventional devices since the air gap also depends on the specimen being flat and smooth. This issue is addressed in the stripline design of Figure 1 by purposely including a dielectric buffer layer at the end of the probe. The buffer layer significantly reduces the sensor's sensitivity to airgap or material flatness. This does come at the cost of some decreased sensitivity; however, the sensitivity decrease is compensated in part by the addition of the flanges at the open end. As will be shown later, even with this buffer layer, the probe sensitivity is sufficient to have good accuracy for most materials of interest.

A photograph of the measurement apparatus with the handle removed is shown in Figure 2. The width of the probe is approximately 10 cm across. The sensor is electrically small at 100 MHz, so a pair of ferrite chokes are integrated into its construction to minimize interference effects from reflected energy that propagates around the outside of the sensor. An RP-10 integrated vector network analyzer, designed by Copper Mountain Technologies, is directly attached to the sensor with an N-type connector. The probe and analyzer can measure reflection amplitude and phase up to 1 GHz.

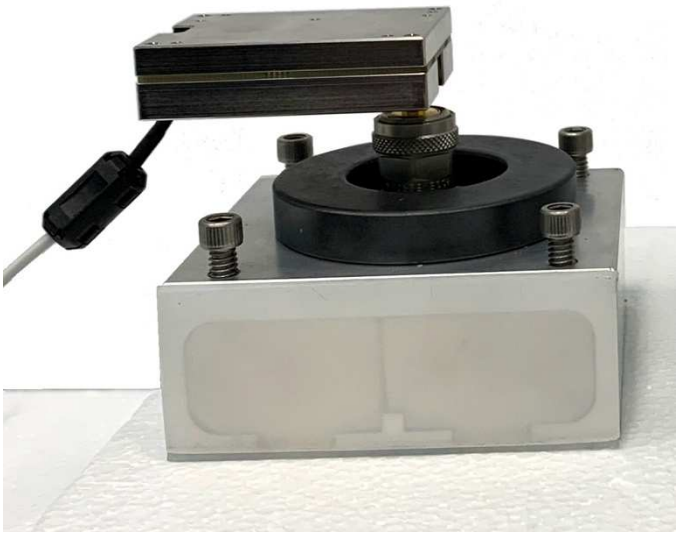

Figure 2. Photograph of open-ended stripline sensor with 1-port vector network analyzer attached.

Examples of the amplitude and phase response for simple acrylic (PMMA) as well as carbon loaded foam are shown in Figure 3. The data in this Figure were calibrated using a simple response method. Traditional low frequency material measurements such as with a waveguide or coaxial airline require multiple calibrations steps. For example, a conventional waveguide will rely on three or more calibration measurements of standards such as opens, shorts, and loads, or sometimes offset shorts. Conventional open-ended coaxial probes similarly employ multiple calibration steps that measure known materials to establish their quantitative calibration. In contrast, the detailed CEM model used for the present sensor enables a much simpler calibration method. Calibration for the data in Figure 3 used just a single calibration measurement of a clear site (no specimen), $S_{11}^{cal} = S_{11}^{specimen} / S_{11}^{clearsite}$. No additional smoothing or time-domain signal process is applied.

In the Figure 3 data, two different thicknesses of acrylic were measured, and they both have little impact on the measured amplitude (top plot). This is expected since acrylic is a simple polymer with not much dielectric loss. However, the effect of varying thickness on the reflection phase is significant (bottom plot), with the thicker, 12.3 mm acrylic showing a greater phase delay across the measurement band compared with the thinner, 3 mm acrylic. The data shown here also include measurement of

a 19 mm thick carbon loaded foam. The carbon is semi-conductive, so its amplitude signal shows significant absorption by the specimen, in contrast to the acrylic.

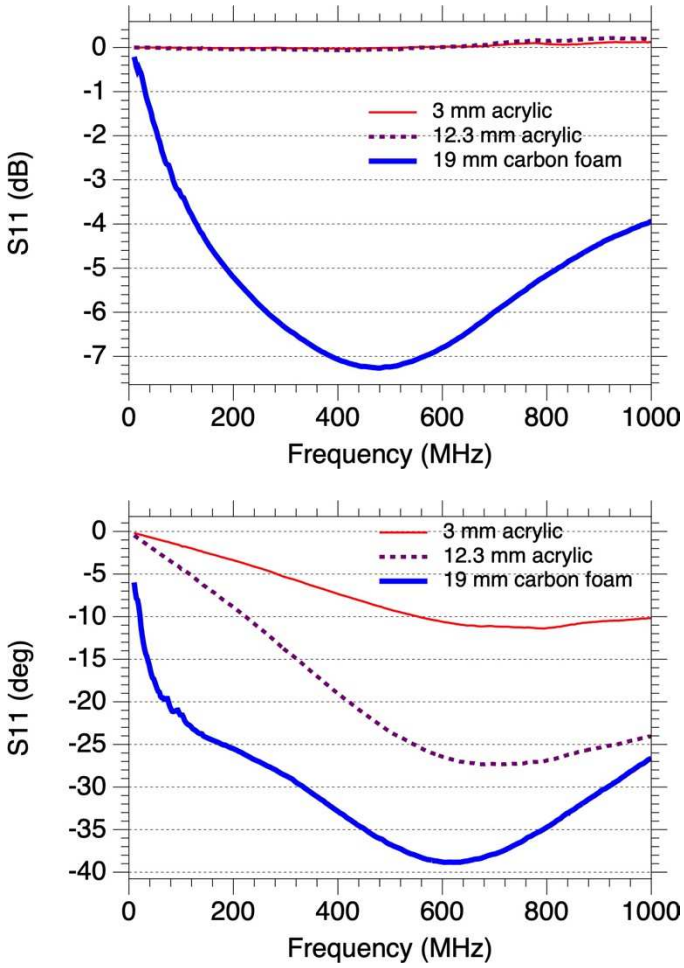

Figure 3. Measured amplitude (top) and phase (bottom) of some acrylic and carbon foam specimens

III. CEM Inversion

For traditional open-ended coaxial probes, analytical expressions based on lumped circuit models can sometimes be used to invert permittivity. This is possible under ideal conditions and where the wavelength is sufficiently low relative to the probe electrical dimensions. Calibration in this case is based on conventional transmission line calibration standards. Conventional open-ended probes have also been used in less ideal situations, where empirical calibration based on known dielectric specimens is required [5]. Empirical calibration is complicated by the need to accurately know the dielectric properties of the calibration standards, which have to have been measured by other methods.

The design of the open stripline probe in Figure 1 precludes any simplistic assumptions that would allow analytical description. Additionally, the idea of empirical calibration with known dielectric standards, while possible, is also not ideal since it depends on having known materials within the range of the unknown specimens and can still be a complicated multi-step process. For this reason, a computational electromagnetic (CEM) inversion method was developed that both overcomes the lack of analytical models and greatly simplifies calibration of the device. With a CEM code, the exact geometry of the probe can be modeled, including details such as radiused corners, connector details, and even the ferrite cores used for interference mitigation.

CEM inversion methods for material property extraction are relatively new since the maturation of full-wave computational electromagnetic tools is also recent. An early example of this method utilized partially filled waveguides with an arbitrarily shaped specimen, which could be modeled with a finite element method [6]. Since then, others have also explored the use of full wave CEM methods for material property inversion [7][8]. These approaches have generally used an optimization scheme to run the full-wave CEM solver iteratively until the best model/measurement match is achieved. Running CEM codes iteratively is time-consuming but effective in a research setting. However it is impractical in other settings since the operation of a CEM code is not straightforward and requires expertise different from that needed to conduct experimenal measurements. Depending on the complexity of the model, the CEM solver can also take significant time to converge to a solution so that rapid measurements and inversions of multiple materials is not possible.

A more practical variation on theis idea of CEM inversion has been succesfully employed in the last few years [4][9]. This modified method, which is also employed in the present work, models the measurement fixture for an array of different intrinsic property combinations and creates a database of CEM results *before* any measurement data is acquired. Once a specimen is measured, the measurement inversion then uses this pre-computed data to find the closest match to the measurement data and applies interpolation to find a more exact solution. Since the time-consuming CEM simulations are all pre-calculated, the inversion calculation is fast and can be applied to measurement data as quickly as it is acquired.

An example of data from this inversion database is shown in Figure 4. Finite difference time domain (FDTD) calculations were run for different combinations of real permittivity, conductivity (which is related to imaginary permittivity), and specimen thickness. This figure is just a portion of the database at 200 MHz and for a specimen thickness of 8 mm. Each pixel in this image corresponds to a separate FDTD simulation. FDTD simulations are conducted in time domain so, the 200 MHz data in Figure 2 was after the FDTD results were converted into frequency domain via a Fourier transform. Each FDTD run provides broad band frequency data, so the calculations necessary for creating the database only need to be iterated for each of the intrinsic parameter and thickness values desired. Similar data is also generated from these runs for probe amplitude.

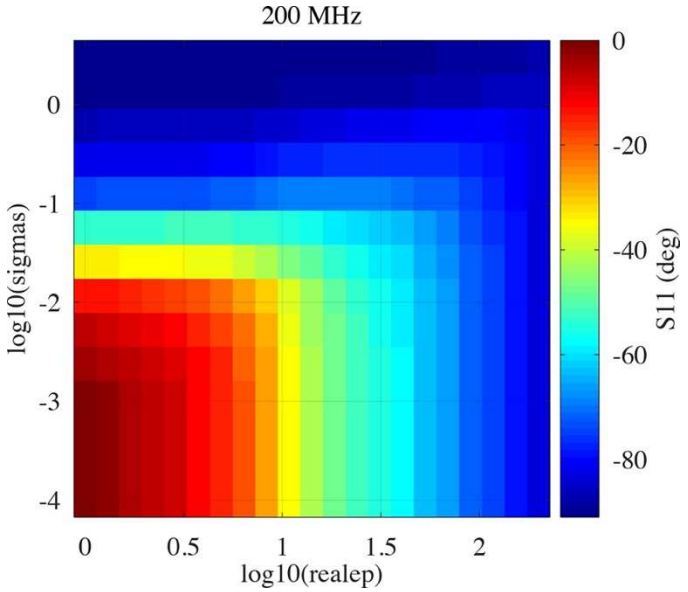

Figure 4. Reflection phase from inversion database at 200 MHz versus permittivity and conductivity.

IV. RMMP Measurements

Using the inversion method described above, Figure 5 shows inverted dielectric permittivity for some simple dielectrics. The real permittivity is plotted as solid lines and the imaginary permittivity as dashed. These materials have an approximately constant real permittivity and an imaginary permittivity near zero. The fiberglass is a non-woven composite, which shows a relative permittivity near 4.2, typical for these types of materials. The acrylic permittivity is from the same two acrylic specimens described in Figure 3 with different thicknesses. The inverted acrylic permittivity is just above $\varepsilon \sim 2.6$, consistent with acrylic or PMMA measurements in the literature [10]. An initial measurement uncertainty can be estimated by assuming the acrylic specimens should have a constant permittivity and loss. With this assumption, the standard deviation of the inverted permittivity across the frequency band is less than +/- 0.03 for the real part and +/- 0.02 for the imaginary part. There are systematic errors this does not account for, and the assumption of constant real and imaginary permittivity may not be completely valid, but it does give a first order-of-magnitude estimate.

Figure 3 also shows the amplitude and phase of a carbon-filled foam absorber, and the corresponding inversion of permittivity is shown in Figure 6. The solid line is the real part, and the dashed line is the imaginary. The x-axis of this plot is logarithmic so that the open stripline sensor results can be shown alongside free-space inverted properties from the same specimen at higher frequencies (3-20 GHz). Carbon-loaded foam is semi-conductive and thus dispersive. Therefore, in this case the comparison can only verify that the low and high frequency data follow the same trends. The real permittivity being relatively low is consistent with foam being a mix of polymer and air. The increasing imaginary permittivity as frequency decreases is characteristic of the conductive carbon providing long-range paths for electron conduction.

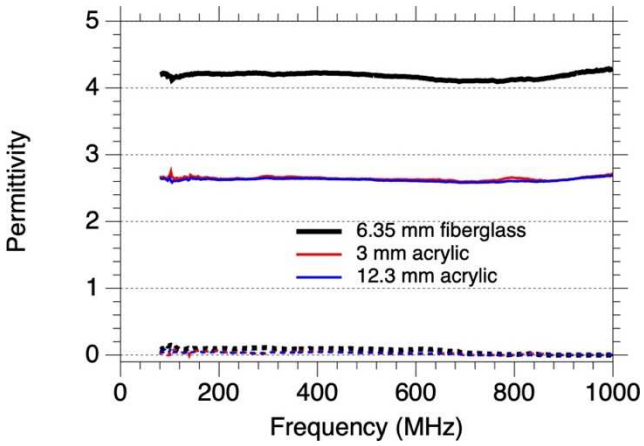

Figure 5. Inverted real (solid) and imaginary (dashed) permittivity from fiberglass and acrylic specimens

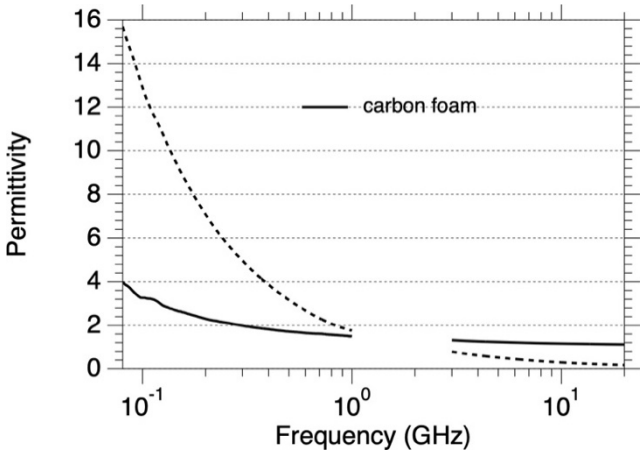

Figure 6. Inverted real (solid) and imaginary (dashed) permittivity from lossy carbon foam

This open-ended probe can be used for thin resistive materials as well. These materials are characterized with a sheet or surface impedance in ohms per square units. The inverted properties in Figure 7 are for two different resistive specimens with different carbon ink coatings. The probe data is compared to WR-4200 waveguide (160 to 350 MHz). The waveguide data were measured by sandwiching an oversized resistive specimen in the flanges between two waveguide sections, and the sheet impedance was inverted from the transmission (S_{21}) data by,

$$Z_s = \frac{Z_0 S_{21}}{2(1-S_{21})} \frac{1}{\sqrt{1-\left(f_c/f\right)^2}}, \quad (1)$$

where f is frequency, f_c is the waveguide cutoff frequency and Z_0 is the impedance of free space.

The cross-section of the WR-4200 waveguide is 42 inches (107 cm) wide, significantly more than the 10 cm stripline probe. Therefore, probe measurements were made at eleven locations across the specimen and averaged to compare to the waveguide.

The averaging also applied a cosine weighting function versus location to account for the electric field variation across the waveguide cross-section. The probe results are within 5 percent or better of the waveguide measurements for the real part and within 10 ohms of the imaginary part, showing good agreement.

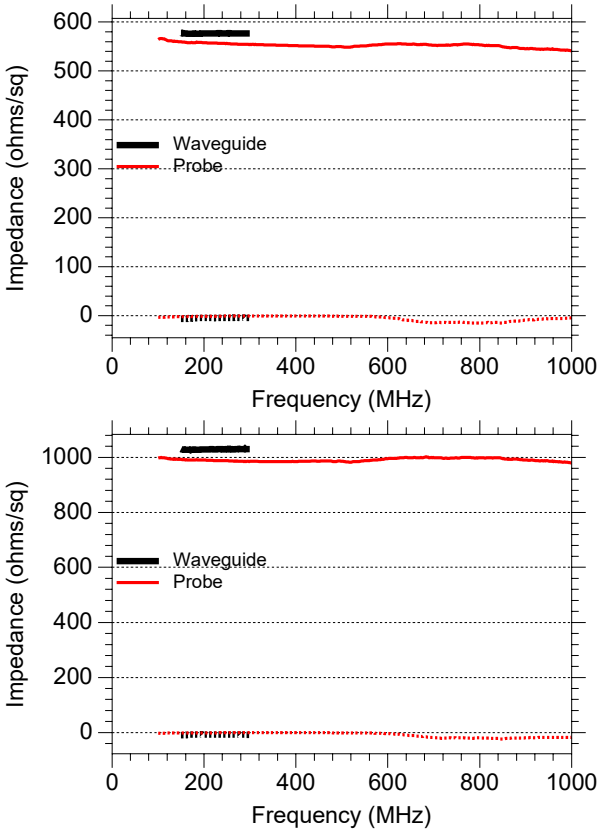

Figure 7. Impedance vs. frequency for two resistive sheets, solid line is real part and dashed line is imaginary.

V. Large Anisotropy Correction

The stripline design of the sensor leads to a preferential polarization axis for the electric field. The electric field of an arbitrarily large sensor would be almost entirely polarized along this axis, but the finite size of the actual sensor results in some cross-polarization leakage at the end of the sensor. This induces a measurement bias for strongly anisotropic materials. An example of this effect is in Figure 8, which shows a simulated example for a 10:1 anisotropy in both the resistance, R, and capacitance, *C*, where the complex impedance, *Z*, is represented as $Z = 1/(1/R + i\omega C)$ and ω is angular frequency. The undesired cross-polarization coupling shifts the inverted impedance ("Apparent") relative to the actual impedance. The dashed and solid curves represent the two orthogonal directions. The cross-polarization leakage is strongest in the higher impedance orientation with errors of roughly 40% and 60% for the real and imaginary components respectively. The low impedance direction is less affected by this error, but still shows an approximately 20% error in the real impedance.

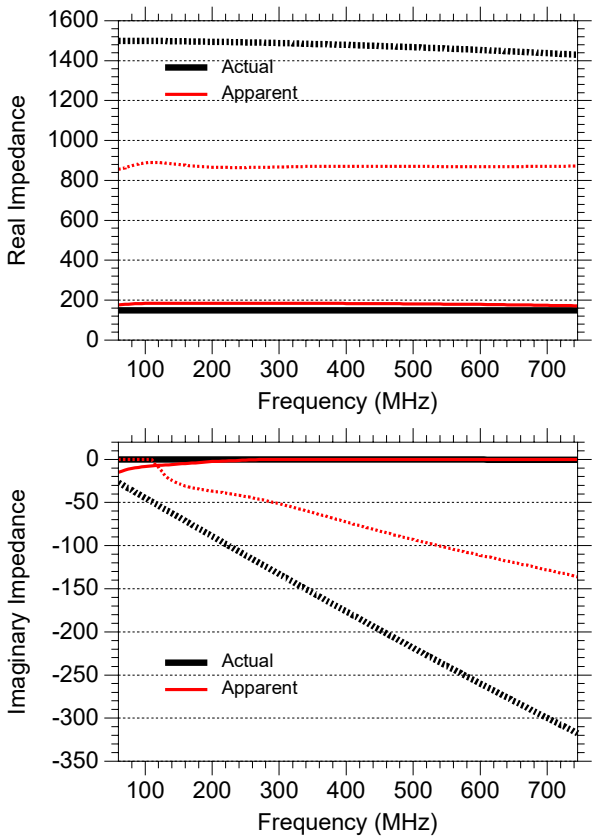

Figure 8. FDTD inversion with 1:10 anisotropy in both R and C. Solid/dashed curves are orthogonal orientations.

To determine polarization leakage, FDTD simulations of anisotropic and isotropic resistive sheets were compared. This work only explored anisotropy in thin impedance sheets, and future research will generalize to bulk materials. The simulated sheets have on-axis (parallel to the primary polarization direction) resistance and capacitance (R_1 and C_1) and a 90-degree off-axis set (R_2 and C_2). So, we define an anisotropy factor for resistance ($a_r = R_1/R_2$) and for capacitance ($a_c = C_1/C_2$). The present work also neglects cross-terms between the resistive and capacitive properties, so that the effect is strictly a function of (R_1, a_r) for resistance and (C_1, a_c) for capacitance. A set of equations can be iteratively solved to correct the inverted resistance and capacitance for the two principal directions at each frequency,

$$m_1\,(1 - a_r) = \frac{r}{r_0} - 1, \tag{2}$$

$$m_2\left(\frac{1}{a_r} - 1\right) = \frac{\frac{1}{r_{inf}} - \frac{1}{r_0}}{\frac{1}{r_{inf}} - \frac{1}{r}} - 1, \tag{3}$$

$$m_3 \ln(a_c) = \frac{c_0}{c} - 1, \tag{4}$$

$$m_4\,(1 - a_c) = \frac{c_0}{c} - 1, \tag{5}$$

where r_0 and c_0 are the true resistance and capacitance of the material in a principal direction at some frequency. r and c are the apparent resistance and capacitance when an isotropic inversion model is assumed and r_{inf} is the apparent resistance

when the off-axis resistance is zero. These equations were derived empirically with the exception of Equation 3, which is a parallel circuit model. For most of the equations, only a single fitting parameter is needed, which allows a sparser set of simulations to build out the coefficient table. For Equation 3, the value of r_{inf} can be directly computed from a single simulation per resistance value.

If the true anisotropy ratios were exactly known, corrected impedance could be obtained from a single orientation along either principal axis. Instead, correction requires measurement of both principal axes to estimate the anisotropy ratio (generally an under-estimate). After applying the estimated correction factor to each of the two measurements, an updated anisotropy ratio is calculated, and this process is repeated until convergence to a stable solution. Figure 9 shows this correction algorithm applied to an example resistive specimen with extremely high anisotropy and compared to waveguide measurement. The correction reduced the deviation of the RMMP data from waveguide data from roughly 60% and 70% to 26% and 10% for the real and imaginary impedances, respectively. The anisotropy ratio in this specimen is estimated to be around 40:1 for resistance and 10:1 for capacitance, which leads to a large correction factor and thus more residual error.

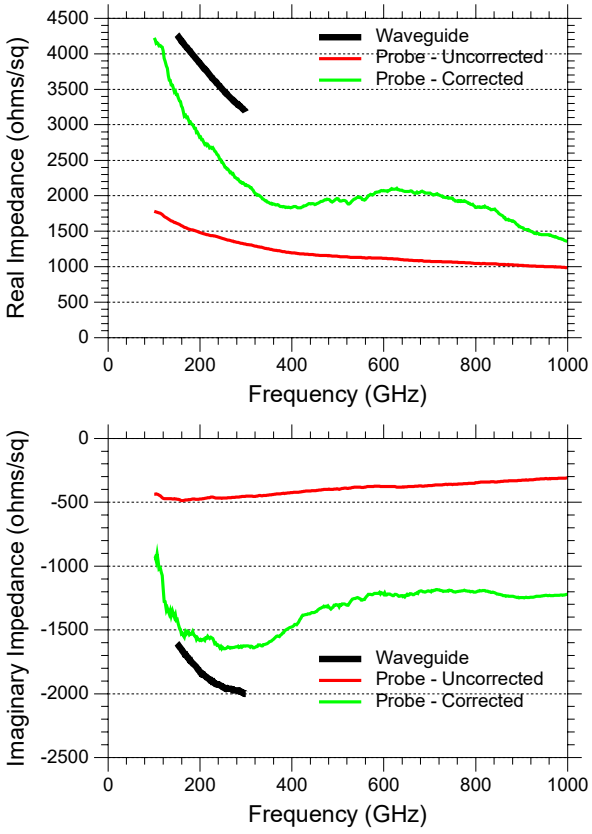

Figure 9. Impedance vs frequency plots for waveguide and RMMP data showing effect of anisotropy correction.

The current anisotropy correction has some simplifying assumptions: 1. cross-terms between resistance and capacitance are excluded, 2. it does not handle positive reactance, 3. it has not been applied to bulk materials, and 4. extremely anisotropic sheets (i.e. more than 20:1 ratio) may require a more sophisticated model. Many of these factors can be addressed by expanding the number of simulation-derived coefficients and increased model complexity, with the cost of more numerous simulations, larger correction table size, and slower computational speed when applying the lookup values.

VI. Conclusion

A new open-ended stripline sensor was presented as a handheld tool for UHF/VHF measurements. This probe was validated for both bulk nonmagnetic materials and thin, impedance sheet materials. The system has comparable accuracy to waveguide measurements (within ~5% for isotropic resistive specimens) while having a smaller footprint, higher bandwidth, and ability to measure materials *in situ*. While the ability of the probe to accurately measure highly anisotropic materials is more limited, an algorithmic correction approach was developed and greatly reduces the error due to polarization leakage.

Acknowledgement

Thanks to Zander Borders, Brenda Negrete, and Maryanne Bohannan for help in measuring material specimens, and thanks to Juan Calzada, Dr. John Welter, and Danielle Kelly at AFRL for their encouragement and support. This work was funded by USAF contract FA8650-21-C-5019.

References

[1] J. Baker-Jarvis, “Transmission / Reflection and Short-Circuit Line Permittivity Measurements,” NIST Technical Note 1341, July 1990

[2] J.W. Schultz, B.P. Petrie, C.L. Bethards, J.G. Maloney, J.G. Calzada, J.T. Welter, “Flat Lens Antenna Technology for Free Space Material Measurements,” Proc. of 2021 AMTA Symposium, October 2021

[3] J.W. Schultz, “A New Dielectric Analyzer for Rapid Measurement of Microwave Substrates up to 6 GHz” Proc. of 2018 AMTA Symposium, October 2018

[4] J.W. Schultz, J.G. Maloney, “A New Method for VHF/UHF Characterization of Anisotropic Dielectric Materials,” Proc. of 2015 AMTA Symposium, November 2015

[5] M.A. Stuchly, S.S. Stuchly, “Coaxial Line Reflection Methods for Measuring Dielectric Properties of Biological Substances at Radio and Microwave Frequencies—A Review,” IEEE Trans on Instrumentation and Measurement, IM-29(3), pp. 176-183, September 1980

[6] M.D. Deshpande, C.J. Reddy, P.I. Tiemsin and R. Cravey, "A new approach to estimate complex permittivity of dielectric materials at microwave frequencies using waveguide measurements," in IEEE Transactions on Microwave Theory and Techniques, vol. 45, no. 3, pp. 359-366, March 1997

[7] M.W. H.IV, J.W. Stewart, M.J. Havrilla, W.P. Baker, E.J. Rothwell and D.P. Nyquist, "Nondestructive electromagnetic material characterization using a dual waveguide probe: A full wave solution," in Radio Science, vol. 44, no. 3, pp. 1-13, June 2009

[8] A.K. Amert and K.W. Whites, "Characterization of small specimens using an integrated computational/measurement technique," 2013 IEEE Antennas and Propagation Society International Symposium (APS/URSI), 2013, pp. 706-707

[9] R. D. Geryak, J. W. Schultz, Z. Borders, J. G. Maloney, J. G. Calzada and J. T. Welter, "New Method for Determining Permittivity of Thin Polymer Sheets," 2021 Antenna Measurement Techniques Association Symposium (AMTA), 2021

[10] B. Riddle, J. Baker-Jarvis, J. Krupka, “Complex Permittivity Measurements of Common Plastics Over Variable Temperatures,” IEEE Trans. Microwave Theory and Techniques, 51(3), 727-733, March 2003